McGrath, S.M., et al., 2023, Pleistocene Sunda Shelf submersion-exposure cycles initiate vegetation Walker Circulation feedback: Geology, https://doi.org/10.1130/G51412.1

Supplemental Material

METHODS

Site Description

IODP Expedition 353 recovered sediment from a rise in the Andaman Sea (eastern Bay of Bengal) Site U1448 (10°38.0'N, 93°00.0'E, 1091mbsl, 44km offshore) (Fig. 1) (Clemens et al., 2016). Terrigenous sediment supply to the Andaman Sea is dominantly from the Irrawaddy River (Colin et al., 1999, 2006) with contributions from the Salween River and Indo-Burman-Arakan mountain ranges as well as the Andaman Islands (Awasthi et al., 2014). U1448 XRF data shows sediment supply is influenced by global sea level changes with more detrital sediment input from rivers during lowstands (Gebregiorgis et al., 2020) and shows no shift or change in sediment composition trends since the initiation of Sunda Shelf submersion-exposure cycles.

Age Model

The age model of Site U1448 is based on two radiocarbon dates, and tie points between benthic foraminifera $\delta^{18}O$ and the LR04 global $\delta^{18}O$ benthic stack (Lisiecki and Raymo, 2005) using AnalySeries (Paillard et al., 1996). Details of the U1448 benthic record and its tie-points to the LR04 global $\delta^{18}O$ benthic stack are detailed in Clemens (2022). For AMS, specimens of upper-ocean planktonic foraminiferal species *Globigerinoides ruber* (white *sensu stricto*) were picked from the 250–355 μm size fraction. Radiocarbon analysis was performed at the Woods Hole Oceanographic Institution National Ocean Sciences Accelerator Mass Spectrometry (WHOI NOSAMS) facility. Each radiocarbon date was calibrated into calendar years using the CALIB Radiocarbon Calibration (Stuiver and Reimer, 1993) using the standard marine reservoir correction and the Marine20 curve (Heaton et al., 2020). Correlations, tie points, radiocarbon dates, and accumulation rates are shown in Supplementary Figure 1 and Supplementary Table 1.

Organic Geochemical Analyses

From the marine sediment, we use terrestrial organic leaf waxes as a regional proxy for vegetation. Leaf wax fatty acids have been shown to have short residence times (from 0.015 to 1.2 kyr) (French et al., 2018; Galy & Eglinton, 2011) that do not interfere with the timing of the forcing and response investigated here. Additionally, in previous orbital scale leaf wax studies within the Bay of Bengal, the phase relationships between the precipitation isotopes recorded from leaf waxes are in phase with the precipitation isotopes recorded in speleothems that have independent, well constrained age models (McGrath et al., 2021).

Lipids are extracted from 3 to 8g of freeze-dried sediment with an Accelerated Solvent Extractor 200 (Dionex) using a 9:1 mixture of dichloromethane: methanol. The extracts are dried under N2 and separated on aminopropyl silica gel flash columns eluting neutral fractions with dichloromethane (DCM): isopropanol 2:1 (v: v) and acid fractions with 4% acetic acid in diethyl ether. All flash column separations use three column volumes of each eluent. The neutral fraction containing the *n*-alkanes are quantified on a GC-FID using an internal standard. The *n*-alkanes average chain length (ACL) is calculated by:

$$ACL = \frac{27\times C_{27}+29\times C_{29}+31\times C_{31}+33\times C_{33}}{C_{27}+C_{29}+C_{31}+C_{33}}. \quad (1)$$

Acid fractions are methylated in anhydrous 5% HCl in methanol at 60°C overnight. Samples are further cleaned using silica gel flash columns: polar compounds are removed with hexane, fatty acid methyl esters (FAMEs) are eluted with DCM. The $\delta^{13}C$ of the *n*-alkanoic acids are measured using Gas Chromatography-Pyrolysis Isotope Ratio Mass Spectrometry at Brown University. Samples are run in duplicate with standards run every 4 injections. The reproducibility of the $\delta^{13}C$ measurement based on repeated analyses was better than ±0.2‰.

Samples have been corrected for the methyl group added during fatty acid derivatization using the known isotopic composition of the acidified methanol used in methylation.

TIMESERIES ANALYSIS METHODOLOGY

We use evolutionary power spectral analysis to assess the time varying amplitude of spectral peaks. We applied the Lomb-Scargle method due to its ability to use unevenly spaced time series. On average, the timeseries analyzed have mean resolution of 2.5 kyr and were assessed over the last 640 kyr or maximum timeseries age with a sliding window length set to 50. We conduct wavelet cross-spectrum analysis to assess the coherence between the U1448 vegetation and various vegetation and SST proxies. Here, timeseries are linearly interpolated to a timestep of 1 kyr over the last 640kyr or maximum timeseries age.

PROXIES FROM THE SOUTH CHINA SEA

Previous studies from sites in the South China Sea have also noted a regime change around 250 ka in vegetation (Li et al., 2015) and runoff (Zhang et al., 2007) associated with a weaker Pacific Walker Circulation. Zhang et al. (2007) found a decline in runoff around 240 ka at ODP Site 1143 (southern South China Sea) which they linked with changes in the Pacific Ocean SST gradient and El Niño-like conditions. Li et al. (2015) created an *n*-alkane record from site MD05-2901 (South China Sea) showing reduced glacial-interglacial variability of ACL around 270 ka, inferred to reflect reduced humidity during glacial periods. While the ACL records at Site U1448 and MD05-2901 show different shifts in variability, the timing and direction of change at both sites support drier glacial conditions associated with weaker Walker Circulation.

MODERN EL NINO - SOUTH ASIAN SUMMER MONSON RELATIONSHIP

In the modern, El Niño is related with weaker South Asian Summer Monson (SASM) causing warmer and drier summer monsoon conditions through the displacement of the Walker Circulation (Sikka, 1980; Webster and Yang, 1992). Over the recent decades, the ENSO-SASM relationship has waxed and waned over Indian subcontinent (Kumar et al., 1999; Yu et al., 2021), however, there has consistently been a strong negative correlation between ENSO and rainfall over the southeast Asian peninsula and maritime continent (Wang et al., 2020). This strong ENSO-SASM-vegetation relationship over Southeast Asian peninsula and maritime continent is apparent in the paleoclimate records. While the CMZ vegetation proxies from U1446 lack the 250 ka vegetation shift (Fig. 2D), the Southeast Asian peninsula vegetation proxies from U1448 and the maritime continent vegetation proxies from MD98-2152 both show a strong ENSO-SASM-vegetation relationship (Fig. 3A, D-F, Fig S3).

Table S1. Depth- age tie points

U1448 CCSFD (m)	Time (kyr)	Accumulation Rate (m/kyr)	Notes
0.01	0.56	0.134	Radiocarbon
0.99	7.90	0.071	Radiocarbon
1.74	18.53	0.107	
2.69	27.34	0.060	
5.25	70.21	0.177	
5.70	72.76	0.580	Toba Ash
6.11	73.48	0.071	
7.09	87.22	0.061	
8.61	112.11	0.056	
9.61	130.11	0.034	
9.76	134.54	0.077	
11.73	160.16	0.113	
14.10	181.16	0.069	
14.78	190.97	0.061	
15.52	203.09	0.056	
16.24	215.91	0.110	
16.61	219.29	0.061	
18.11	243.88	0.083	
19.96	266.11	0.055	
21.02	285.13	0.060	
21.57	294.26	0.032	
22.28	316.92	0.053	
23.47	339.32	0.090	
24.83	354.48	0.039	
26.39	394.67	0.049	
28.21	431.54	0.109	
29.88	446.80	0.029	
30.61	471.80	0.065	
32.13	495.34	0.035	
32.70	511.75	0.061	
33.98	532.50	0.042	
34.78	551.64	0.048	
36.06	578.33	0.063	
36.47	584.85	0.056	
36.90	592.54	0.046	
38.25	621.67	0.088	
38.65	626.19	0.049	

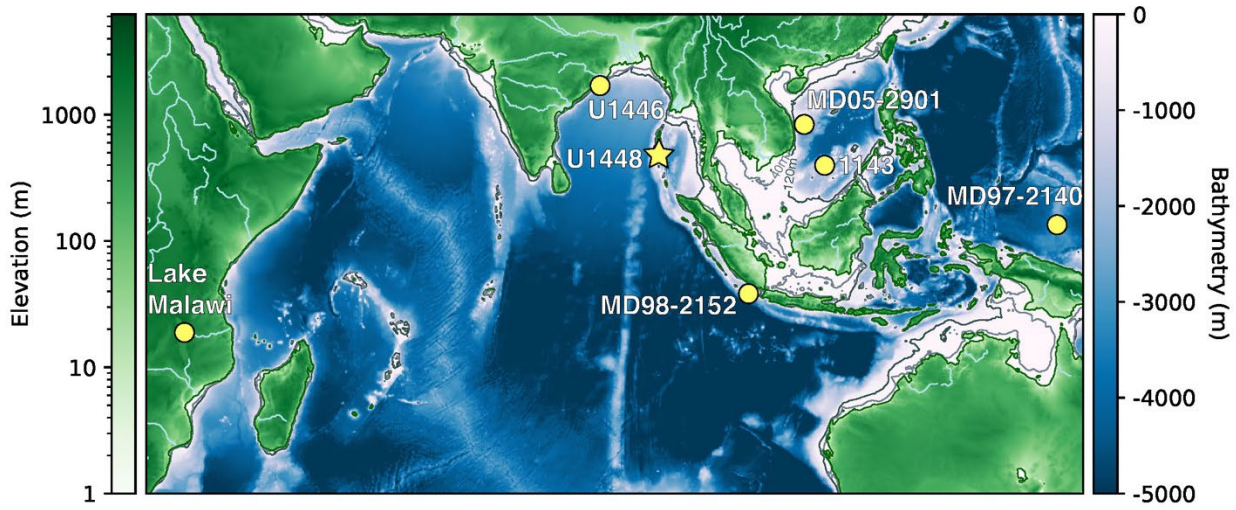

Figure S1. Bathymetry and elevation map. Yellow star marks Site U1448. Yellow circles mark Site U1446, MD98-2152, ODP Site 1143, MD05-2901 and MD97-2140. ODP Site 846 (3° 5' S, 90° 49' W) is in the eastern equatorial Pacific Ocean cold tongue. Base map from GeoMapApp (Ryan et al., 2009) with grey lines indicating 40m and 120m isobaths.

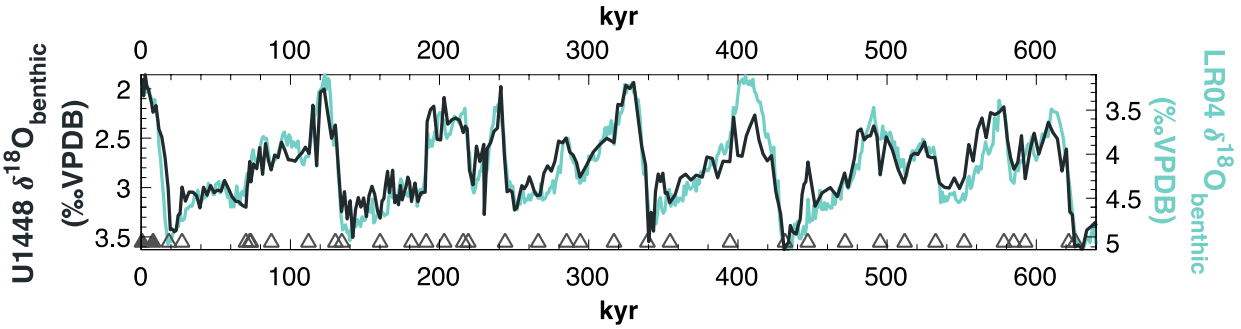

Figure S2. U1448 benthic $\delta^{18}O$ Clemens (2022) stratigraphy overlays the LR04 stack (Lisiecki and Raymo, 2005) with closed triangles indicating radiocarbon dates and open triangles indicating tie points.

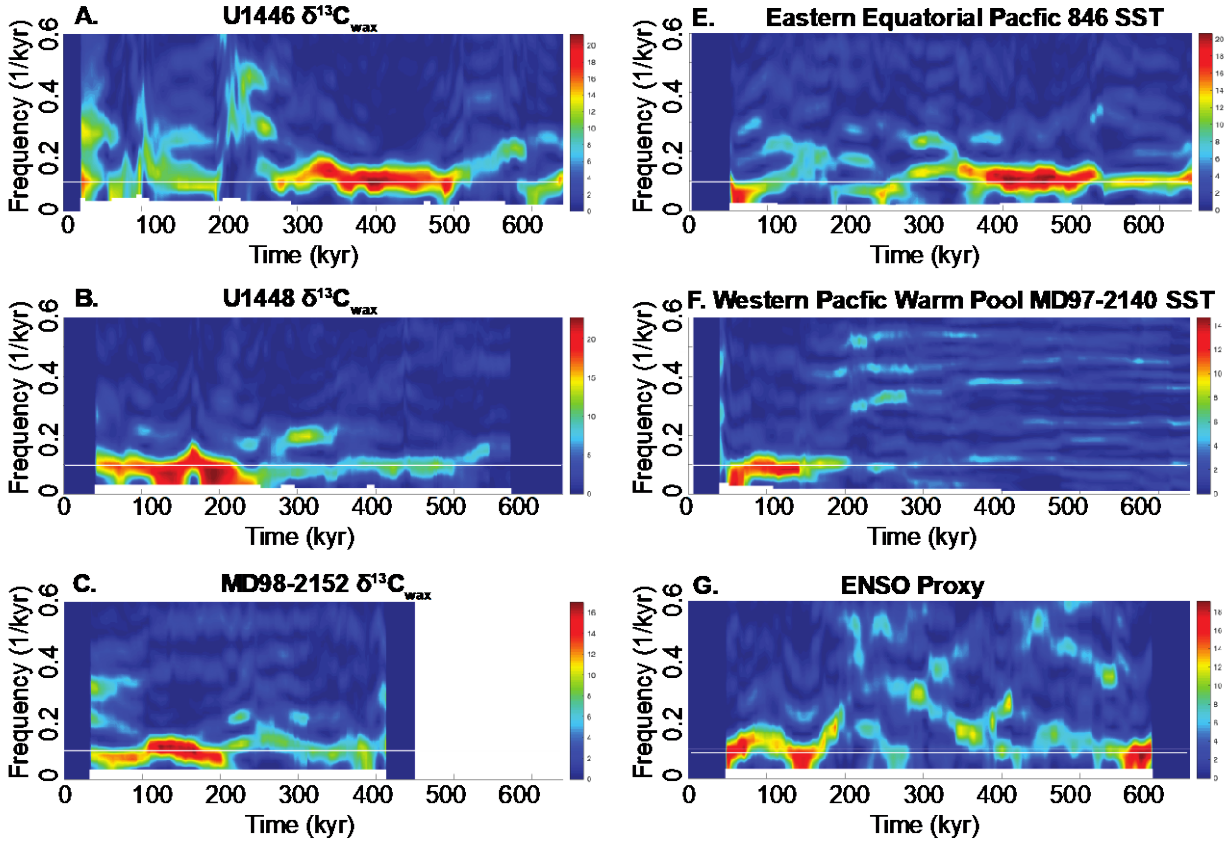

Figure S3. Evolutionary Lombe-Scargle power spectrums: A) U1446 $\delta^{13}C_{wax}$ (Yamamoto et al., 2022), B) U1448 $\delta^{13}C_{wax}$, C) MD98-2152 $\delta^{13}C_{wax}$ (Windler et al., 2019), E) ODP Site 846 SST (Liu and Herbert, 2004), F) MD97-2140 SST (De Garidel-Thoron et al., 2005), G) ENSO proxy based on the difference of western Pacific warm pool site MD98-2140 minus eastern Pacific ODP Site 846 SST. White line at 0.01 indicate glacial-interglacial 100 kyr power.

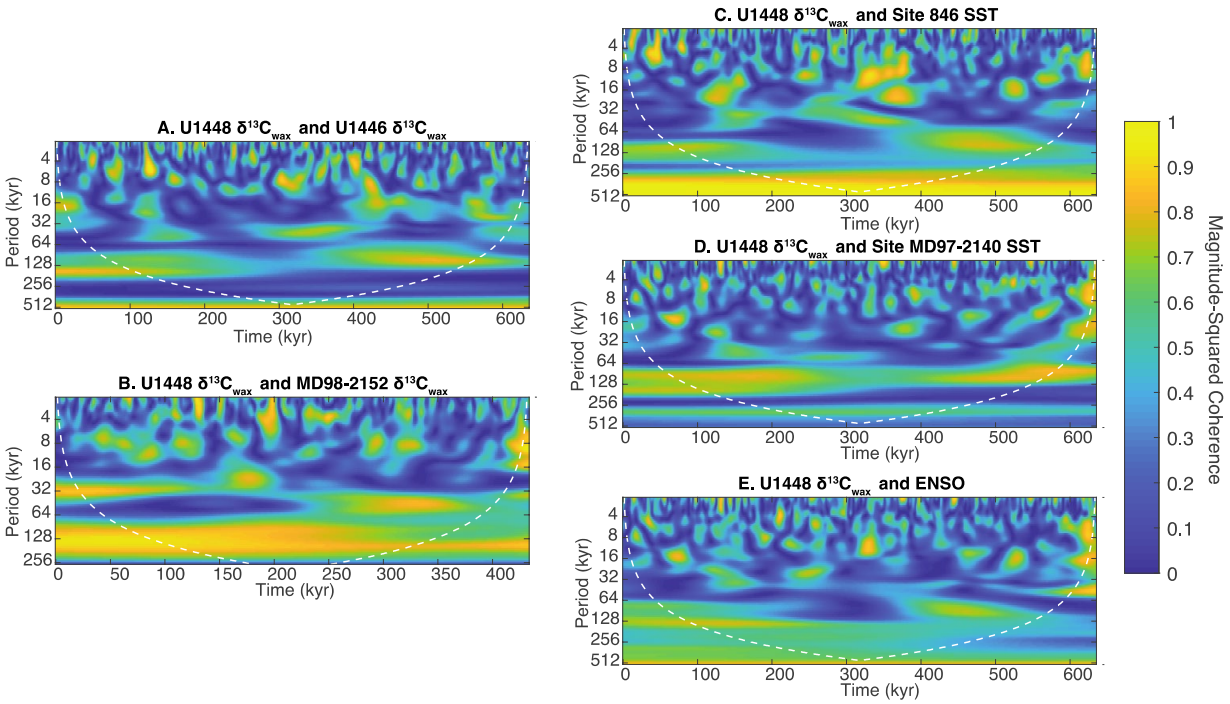

Figure S4. Wavelet Coherence: U1448 $\delta^{13}C_{wax}$ vs, A) U1446 $\delta^{13}C_{wax}$ (Yamamoto et al., 2022), B) MD98-2152 $\delta^{13}C_{wax}$ (Windler et al., 2019), C) ODP Site 846 SST (Liu and Herbert, 2004), D) MD97-2140 SST (De Garidel-Thoron et al., 2005), E) the difference of western Pacific warm pool site MD98-2140 minus eastern Pacific ODP Site 846 SST.

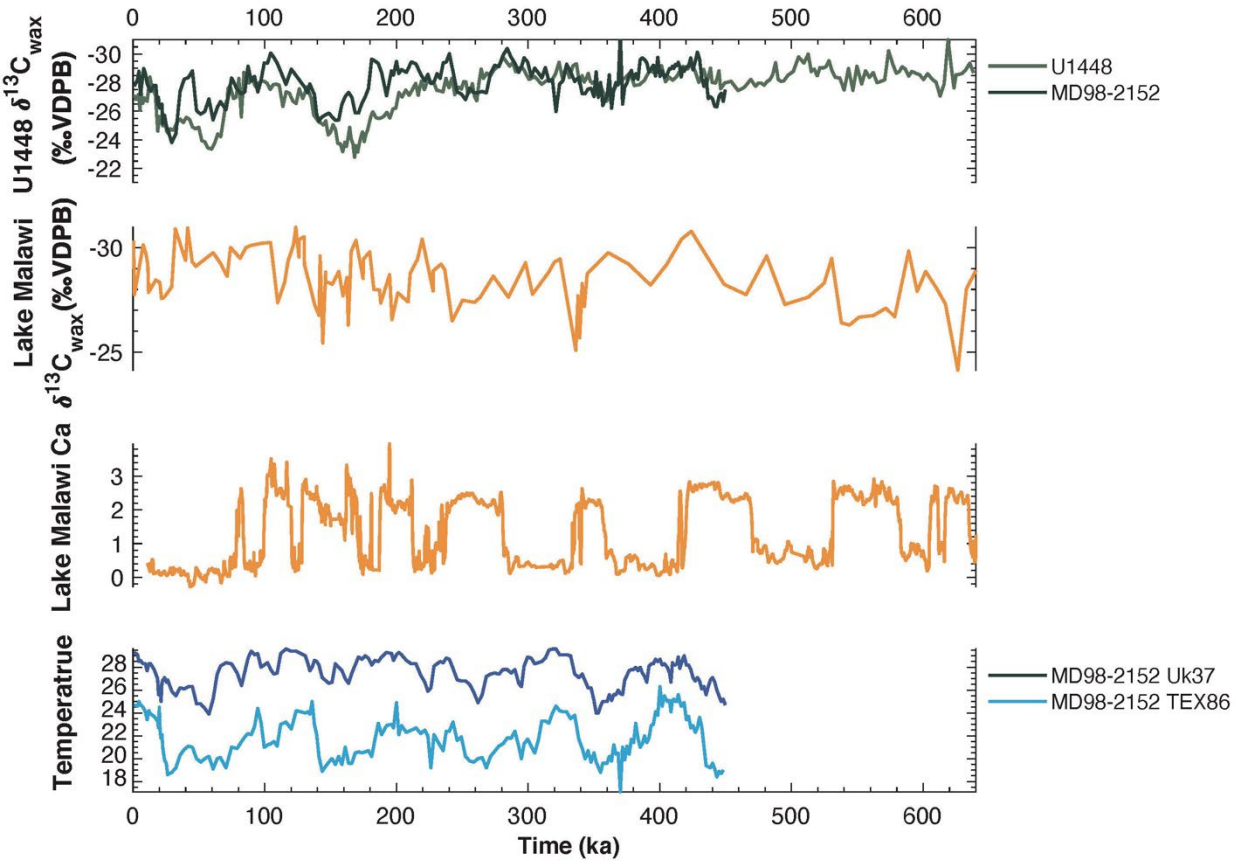

Figure S5. Southeast Asia Vegetation relationship with the Indian Ocean Walker Circulation. From top to bottom: Southeast Asia $\delta^{13}C_{wax}$, Lake Malawi $\delta^{13}C_{wax}$ (Johnson et al., 2016), Lake Malawi Ca (Johnson et al., 2016), and sea surface and thermocline temperature MD98-2152 (Windler et al., 2019).

REFERENCES CITED

Awasthi, N., Ray, J.S., Singh, A.K., Band, S.T., and Rai, V.K., 2014,Provenance of the Late Quaternary sediments in the Andaman Sea: Implications for monsoon variability and ocean circulation: Geochemistry, Geophysics, Geosystems, v. 15, p. 3890–3906, https://doi.org/10.1002/2014GC005462.

Clemens, S.C., 2022, Data report: Site U1448 Pleistocene benthic foraminiferal stable isotopes, Andaman Sea, IODP Expedition 353, *in* Clemens, S.C., et al., eds., Indian Monsoon Rainfall: Proceedings of the International Ocean Discovery Program, Volume 353: College Station, Texas, International Ocean Discovery Program, https://doi.org/10.14379/iodp.proc.353.203.2022

Clemens, S.C., et al., 2016, Site U1448: Indian Monsoon Rainfall: Proceedings of the International Ocean Discovery Program, Volume 353: College Station, Texas, International Ocean Discovery Program, https://doi.org/10.14379/iodp.proc.353.108.2016.

Colin, C., Turpin, L., Bertaux, J., Desprairies, A., and Kissel, C., 1999, Erosional history of the Himalayan and Burman ranges during the last two glacial–interglacial cycles: Earth and Planetary Science Letters, v. 171, p. 647–660, https://doi.org/10.1016/S0012-821X(99)00184-3.

Colin, C., Turpin, L., Blamart, D., Frank, N., Kissel, C., and Duchamp, S., 2006, Evolution of weathering patterns in the Indo-Burman Ranges over the last 280 kyr: Effects of sediment provenance on $^{87}Sr/^{86}Sr$ ratios tracer: Geochemistry, Geophysics, Geosystems, v. 7, Q03007, https://doi.org/10.1029/2005GC000962.

Gebregiorgis, D., Giosan, L., Hathorne, E.C., Anand, P., Nilsson-Kerr, K., Plass, A., Lückge, A., Clemens, S.C., and Frank, M., 2020, What can we learn from X-ray fluorescence core scanning data?: A paleomonsoon case study: Geochemistry, Geophysics, Geosystems, v. 21, https://doi.org/10.1029/2019GC008414.

Kumar, K.K., Rajagopalan, B., and Cane, M.A., 1999, On the weakening relationship between the Indian Monsoon and ENSO: Science, v. 284, p. 2156–2159, https://doi.org/10.1126/science.284.5423.2156.

Li, L., Li, Q., Li, J., Wang, H., Dong, L., Huang, Y., and Wang, P., 2015, A hydroclimate regime shift around 270 ka in the western tropical Pacific inferred from a late Quaternary n-alkane chain-length record: Palaeogeography, Palaeoclimatology, Palaeoecology, v. 427, p. 79–88, https://doi.org/10.1016/j.palaeo.2015.03.025.

Lisiecki, L.E., and Raymo, M.E., 2005, A Pliocene-Pleistocene stack of 57 globally distributed benthic δ18O records: Paleoceanography, v. 20, PA1003,https://doi.org/10.1029/2004PA001071.

McGrath, S.M., Clemens, S.C., Huang, Y., and Yamamoto, M., 2021, Greenhouse gas and ice volume drive Pleistocene Indian Summer Monsoon precipitation isotope variability: Geophysical Research Letters, v. 48, https://doi.org/10.1029/2020GL092249.

Paillard, D., Labeyrie, L., and Yiou, P., 1996, Macintosh Program performs time-series analysis: Eos (Washington, D.C.), v. 77, p. 379–379, https://doi.org/10.1029/96EO00259.

Ryan, W.B.F., et al., 2009, Global Multi-Resolution Topography synthesis: Geochemistry, Geophysics, Geosystems, v. 10, Q03014, https://doi.org/10.1029/2008GC002332.

Sikka, D.R., 1980, Some aspects of the large scale fluctuations of summer monsoon rainfall over India in relation to fluctuations in the planetary and regional scale circulation

parameters: Proceedings of the Indian Academy of Sciences–Earth and Planetary Sciences, v. 89, p. 179–195, https://doi.org/10.1007/BF02913749.

Wang, B., Luo, X., and Liu, J., 2020, How robust is the Asian precipitation-ENSO relationship during the Industrial Warming Period (1901–2017)?: Journal of Climate, v. 33, p. 2779–2792, https://doi.org/10.1175/JCLI-D-19-0630.1.

Webster, P.J., and Yang, S., 1992, Monsoon and ENSO: selectively interactive systems: Quarterly Journal of the Royal Meteorological Society, v. 118, p. 877–926, https://doi.org/10.1002/qj.49711850705.

Yu, S.Y., Fan, L., Zhang, Y., Zheng, X.T., and Li, Z., 2021, Reexamining the Indian Summer Monsoon rainfall–ENSO relationship from its recovery in the 21st Century: Role of the Indian Ocean SST anomaly associated with types of ENSO evolution: Geophysical Research Letters, v. 48, https://doi.org/10.1029/2021GL092873.

Zhang, Y.G., Ji, J., Balsam, W.L., Liu, L., and Chen, J., 2007, High-resolution hematite and goethite records from ODP 1143, South China Sea: Co-evolution of monsoonal precipitation and El Niño over the past 600,000 years: Earth and Planetary Science Letters, v. 264, p. 136–150, https://doi.org/10.1016/j.epsl.2007.09.022.